Green Chemistry

PAPER

View Article Online
View Journal | View Issue

Cite this: *Green Chem.*, 2025, **27**, 4732

Pollen-templated bio-TS-1: a sustainable catalyst with hierarchical porosity for propylene epoxidation†

Shaodi Sun,‡ Yichen Liao,‡ Zhuang Wang, Chuanhu Wang and Daohua Sun *

Received 4th November 2024,
Accepted 21st March 2025

DOI: 10.1039/d4gc05612d

rsc.li/greenchem

Titanium silicalite (TS-1) emerges as a pivotal catalyst, finding widespread application across the domains of petrochemical and specialty chemical industries. However, its singular microporous structure limits its application in numerous reactions, such as propylene epoxidation. Here, we introduce a N self-doped bio-TS-1 catalyst with a stratified porous structure synthesized using an environmentally friendly pollen templating method. The unique hierarchical porous structure of the bio-TS-1 catalyst optimizes mass transfer efficiency, accelerates product resolution, and prevents the occurrence of carbon deposition. Concurrently, biomass self-doping of nitrogen effectively modulates the electronic structure of the catalyst, with Ti sites being more relaxed and the α-O in Ti-OOH being more aggressive towards C=C bonds of propylene. The synergistic effect breaks the trade-off between performance and stability, with not only the PO yield reaching up to 305 g_{PO} h^{-1} kg_{cat}^{-1} but also the catalyst exhibiting stability for over 120 h. This simplified synthesis strategy provides a feasible solution for the preparation of highly efficient and stable hierarchical porous TS-1-based catalysts.

Green foundation

1. This work introduces an epoxidation catalyst based on the biotemplating method, facilitating the H_2/O_2 route as an alternative to the existing environmentally hazardous production routes.
2. Utilizing the hierarchical porous structure of pollen, the use of additional organic structure-directing agents is eliminated, thereby minimizing the generation of toxic by-products and waste to the greatest extent. Meanwhile, the research objective of enhancing the stability of the catalyst is achieved.
3. The synthesis process free of organic templates by utilizing biological resources holds significant research importance.

1. Introduction

Propylene oxide (PO), recognized as the third most significant propylene derivative and celebrated for its status as a chemical intermediate of significant economic value, is a key player in the chemical industry's production landscape. The direct epoxidation of propylene using hydrogen (H_2) and oxygen (O_2) has long been heralded as the ideal synthesis route for PO, due to its inherent cleanliness, simplicity, and exceptional selectivity.[1–4] In the past decade, the exploration of Au/TS-1 catalysts has intensified, driven by their remarkable efficacy in the vapor-phase epoxidation of propylene.[5–7] However, TS-1 has a microporous structure (0.55 nm) when prepared by the conventional method. The generated PO is difficult to desorb and tends to undergo ring-opening reactions to form byproducts that accumulate on the catalyst surface. Carbon deposits block the pore channels, preventing reactants from entering the pores to react with Au and causing catalyst deactivation.[6,8,9]

TS-1 with a hierarchical pore structure has been reported to reduce the diffusion length for products in zeolites, thereby enhancing its catalytic efficiency.[10–12] For example, Feng *et al.* introduced CTAB as a template and synthesized mesoporous HTS-1, and the enhanced mass transfer ability effectively mitigates side reactions and catalyst deactivation, which are typically induced by the obstruction of micropores.[13] Yu *et al.* have successfully developed a hierarchical porous TS-1 zeolite through an innovative amino acid-assisted synthesis technique.[14] The resulting zeolite features a complex network of inter- and intracrystalline mesopores and macropores, which facilitates the enhanced diffusion of both reactants and products.

Compared to traditional organic template methods, the green synthesis of mesoporous TS-1 has attracted considerable

---

Department of Chemical and Biochemical Engineering, College of Chemistry and Chemical Engineering, Xiamen University, Xiamen 361005, PR China. E-mail: sdaohua@xmu.edu.cn

† Electronic supplementary information (ESI) available. See DOI: **https://doi.org/10.1039/d4gc05612d**

‡ These authors contributed equally.

attention from researchers. This approach dramatically reduces the reliance on hazardous organic structure-directing agents, thereby minimizing the generation of toxic byproducts and waste. The use of renewable and abundant natural biomaterials not only aligns with the sustainability goals of modern chemical processes but also offers substantial economic benefits.[15–18] Among various biological templates, pollen has received much attention as an inexpensive natural product with a unique pore structure and good thermal stability and mechanical strength.[17,19,20] In addition, pollen contains a large amount of N element, which can be used as a template to synchronize elemental doping during the preparation of catalysts to promote the target reaction. For instance, Zhao *et al.* have developed a novel synthesis strategy for N,P co-doped porous 3D-C skeleton@TiO_2 nanoparticles utilizing pollen as a natural template.[21] The incorporation of N and P into the composite material not only enhances its electrical conductivity but also introduces beneficial defects into the carbon framework. It is noteworthy that the majority of existing literature studies concentrate on utilizing pollen as a template for the synthesis of metal oxides, whereas the use of pollen templates in zeolite preparation is seldom documented. How to regulate the crystallization process to induce the zeolite to grow uniformly on the pollen template still needs to be further explored. In addition, it is still a challenge to produce TS-1 zeolite with a special microstructure and effective elemental doping at the same time.

In this work, drawing inspiration from the intricate hierarchical porous structures found in natural biomass, we have employed environmentally benign rape pollen as a template for the synthesis of bio-TS-1 with unique structural features. Comprehensive characterization studies have demonstrated that the bio-TS-1 catalyst possesses a hierarchical porous architecture, and the intrinsic electronic properties of the catalyst are notably modulated by N doping. *In situ* diffuse reflectance infrared Fourier transform spectroscopy (*in situ* DRIFTs) and breakthrough curves have elucidated the distinct influence exerted by the hierarchical pore structure on the mass transfer dynamics. In addition, quasi *in situ* Raman spectroscopy and theoretical calculations have revealed that the Ti sites are more relaxed and the α-O in Ti-OOH is more aggressive towards C= bonds of propylene. The synergistic effect breaks the trade-off between performance and stability. The Au/bio-TS-1 catalyst (305 g_{PO} h^{-1} $kg_{cat}{}^{-1}$) exhibits nearly double the PO formation rate compared to the Au/TS-1 catalyst (176 g_{PO} h^{-1} $kg_{cat}{}^{-1}$), along with higher stability for over 120 h.

2. Experimental section

2.1 Catalyst preparation

Initially, 20 g of rape pollen was subjected to a purification process by washing it thrice in 200 mL of ethanol to eliminate surface contaminants. Subsequently, the pollen was dried at a temperature of 60 °C for a duration of 12 h to obtain pretreated pollen. The synthesis of the bio-TS-1 carrier commenced by preparing a solution where 1.8 mL of Tween 20 was incorporated into 35 mL of deionized water and agitated at 35 °C for 5 minutes. This was followed by the introduction of 12.7 mL of tetrapropylammonium hydroxide (TPAOH) solution, with continued stirring for another 5 minutes. Thereafter, 24.6 mL of tetraethyl orthosilicate (TEOS) solution was added dropwise over a period of approximately 60 minutes, and the mixture was stirred for an additional hour to achieve a clear and transparent solution. In a separate step, 1.1 mL of tetrabutyl titanate (TBOT) was dissolved in 20 mL of isopropanol and then added dropwise to the aforementioned solution. The mixture was further enhanced by the addition of another 4.6 mL of TPAOH solution, which was thoroughly mixed under vigorous stirring. Finally, 6.3 g of the pre-treated pollen was incorporated into the mixture and stirred continuously for 2 h. Upon completion of the stirring process, the resultant mixture was transferred to a sealed Teflon-lined autoclave and subjected to hydrothermal treatment at 170 °C for 48 h. After crystallization, the solid product was extensively washed with deionized water and dried at 80 °C for 12 h. The final step involved calcination of the dried product at 550 °C for 5 h to yield the bio-TS-1 carrier. For comparative analysis, a control sample of TS-1 was synthesized using an analogous procedure, omitting the addition of the biotemplate, with all other steps being identical. The Au loading methodology was adapted from our preceding studies, yielding samples designated as Au/bio-TS-1 for the biotemplate-assisted zeolite and Au/TS-1 for the conventional zeolite.[22] See the ESI† for details on chemicals and materials.

2.2 Characterization studies

X-ray diffraction (XRD), Fourier transform infrared (FTIR) spectroscopy, *in situ* DRIFTS and other characterization studies were performed to analyze the samples in detail, to deepen the understanding of their physicochemical properties and to further explore the reaction mechanism with the characterization results. Specific details of the tests are shown in the ESI.†

2.3 Catalyst evaluation

The catalytic reactions were conducted in a fixed-bed reactor setup. Detailed operational protocols and the relevant calculation methodologies are delineated in the ESI.†

2.4 DFT calculation method

The theoretical calculations were carried out with the Vienna *Ab initio* Simulation Package (VASP).[23] The structures of bio-TS-1 and conventional TS-1 were simulated with a 5 SiO_4 tetrahedral cluster extracted from the typical MFI zeolite at certain locations according to the previous study.[24,25] To elucidate the physicochemical properties of Ti-incorporated zeolite, we substituted a Si atom with a Ti atom, and the peripheral Si atoms were saturated with H atoms along the original Si–O direction. Additionally, one O atom of bio-TS-1 was replaced with a –NH group for subsequent calculations. The as-mentioned Si–H bonds were deliberately constrained to maintain the zeolite topology during the calculations. We employed the projected augmented wave (PAW) method to describe the electron–core interaction with a 400 eV cutoff energy. The exchange–correlation energy was estimated using generalized gradient approximation (GGA) with the Perdew–Burke–Ernzerhof (PBE) functional.[26] For electronic structure calculations, Brillouin zone integration in a 3 × 3 × 1 Monkhorst–Pack grid was set up during the optimization step and a 4 × 4 × 4 grid for electron localization function (ELF) calculation.[27,28] To obtain a relatively accurate result, 10^{-6} eV was introduced for electronic optimization convergence and 0.01 eV $Å^{-1}$ was set for the minimum force threshold during the structural optimization. As for post-processing, we used VESTA for visualization and the VASPKIT code for data analysis.[29]

3 Results and discussion

3.1 Morphological and structural analysis

The synthesis process of bio-TS-1 is depicted in Fig. 1a. Initially, pretreated pollen was incorporated into a prepared TS-1 precursor solution, where it underwent a series of controlled transformations: (1) impregnation to initiate the formation of precursors, (2) hydrothermal reaction to establish the zeolite framework, and (3) calcination to remove organic components. These controlled transformations culminated in the production of the bio-TS-1 zeolite carrier. As shown in Fig. 1b–d, pollen is in the form of a yellow powder. Under microscopic observation, the untreated pollen grains exhibit an elliptical morphology, featuring a complex network of porous surfaces and walls that exhibit open, interconnected porosity.[30] In contrast, the original TS-1 is characterized by its white powder form and homogeneous spherical particles with an average diameter of 200 nm, as shown in Fig. 1e–g.[31] Utilizing a nanocasting approach with raw pollen as a hard template, the macroscopic appearance of bio-TS-1 remains similar to that of TS-1 (Fig. 1h). However, SEM reveals that bio-TS-1 exhibits elliptical particles, approximately 9 × 10 μm in size, resembling the pollen template. This similarity is attributed to the thorough impregnation of the TS-1 precursor solution on the pollen template, leading to nucleation and crystal growth on the template surface during the crystallization process, as observed in Fig. 1i and j.

The XRD patterns for bio-TS-1 and TS-1 samples, as illustrated in Fig. 2a, exhibit comparable diffraction peaks at 2θ values of 7.9°, 8.8°, 23.1°, 23.9°, and 24.3°. The observed peaks

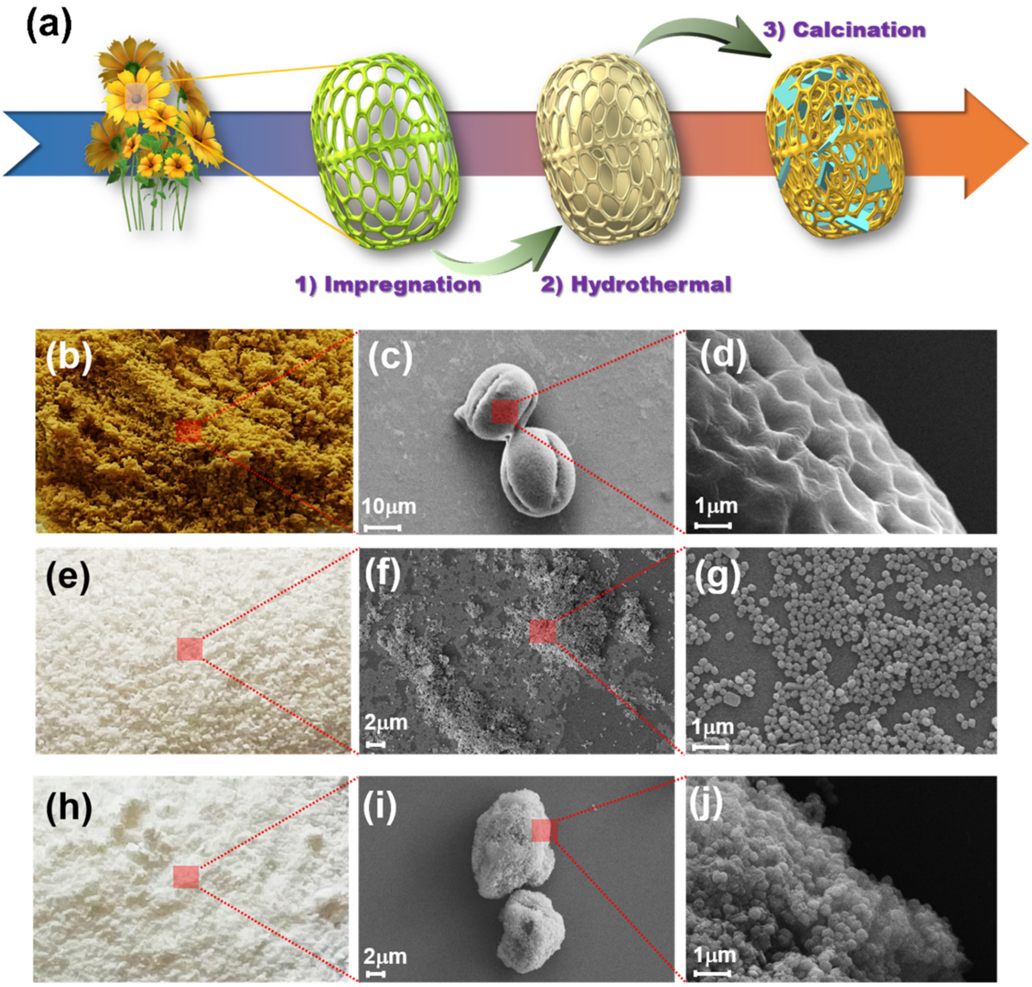

Fig. 1 (a) Schematic illustration of the synthesis of bio-TS-1. Digital photos and representative SEM images of (b–d) pollen, (e–g) TS-1 and (h–j) bio-TS-1.

align with the characteristic diffraction pattern of the MFI zeolite framework, thereby validating the feasibility of the pollen template synthesis strategy.[32] The lack of significant changes in the peak shape after Au loading indicates that the Au particles are small in size and have a high dispersion (Fig. S1†). In the FTIR spectra depicted in Fig. 2b, both bio-TS-1 and TS-1 exhibit characteristic vibrational bands at 1230, 960, 800, and 550 cm^{-1}, which are assignable to the MFI zeolite framework.[33] Typically, the intensity ratio of the peak at 960 cm^{-1} to that at 800 cm^{-1} is used as an indicator of Ti content in zeolites. Specifically, the bio-TS-1 catalyst demonstrates a higher ratio of 0.53, surpassing the TS-1 catalyst's ratio of 0.39. This enhanced ratio suggests that the pollen template method effectively enhances the integration of Ti atoms within the zeolite framework. Furthermore, UV-Raman spectroscopy was employed to probe the structure of the catalyst. As shown in Fig. S2,† the peaks at 380, 800, and 960 cm^{-1} are attributed to the topological structure of MFI, indicating that the addition of pollen did not affect the crystalline structure of the zeolite. Notably, the tetrahedral Ti signals of bio-TS-1 (490, 530, and 1125 cm^{-1}) were significantly stronger than those of TS-1, which is consistent with the infrared results.[34] As shown in the diffuse reflectance ultraviolet-visible spectra (DR-UV vis) in Fig. 2c, both TS-1 and bio-TS-1 exhibit a pronounced absorption peak at 210 nm, indicative of the presence of framework Ti species in tetrahedral coordination. The absence of peaks at 330 nm, which are characteristic of anatase TiO_2, corroborates that only tetrahedrally coordinated titanium is incorporated into the skeletal structure of both materials.[35] After loading Au, a broad peak appeared at 530 nm, which is attributed to the signal of Au (Fig. S3†).[22] However, the state of the Ti species did not change significantly, remaining as isolated framework Ti. The N_2 adsorption–desorption isotherms in Fig. 2d show a steep initial adsorption at P/P_0 below 0.02, confirming the presence of micropores.[36] However, the bio-TS-1 exhibits characteristic type IV isotherms and a H4 hysteresis loop (P/P_0 = 0.7 to 1.0), indicative of the presence of mesopores.[11,13,36] The pore size distribution, in conjunction with these isotherms, suggests an average mesopore diameter of approximately 24 nm for bio-TS-1 (Fig. 2e). Moreover, the mesopore volume (V_{meso}) of bio-TS-1 is 0.52 cm^3 g^{-1}, which is much higher than that of TS-1 (0.27 cm^3 g^{-1}) (Table S1†).[13]

In summary, these findings validate the successful synthesis of the TS-1 zeolite utilizing pollen templates. The incorporation of the pollen template does not alter the crystalline structure or the framework titanium species within the zeolite. However, it significantly modifies the pore architecture of bio-TS-1, leading to the formation of abundant intergranular mesopores. In conjunction with SEM images, it is deduced that the hierarchical pore system of bio-TS-1 is derived from the intrinsic micropores of the zeolite framework, mesopores associated with intergranular voids or defects within the zeolite layers, and the macroporous structure inherited from the original biomass.

3.2 Electronic structure analysis

Not only the pore architecture transformation, but also the influence of pollen on modifying the electronic structure

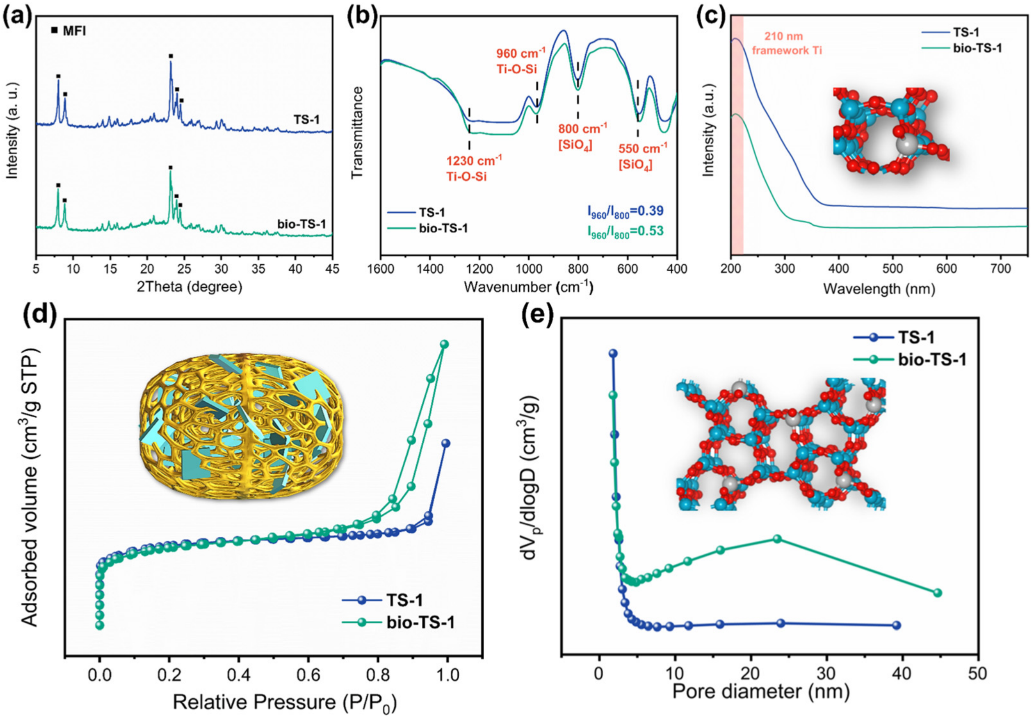

Fig. 2 (a) XRD patterns, (b) FTIR spectra, (c) DR-UV spectra, (d) N_2 adsorption–desorption isotherms, and (e) pore-size distributions based on BJH adsorption of TS-1 and bio-TS-1.

merits careful examination. As illustrated in the Ti 2p XPS spectra depicted in Fig. 3a and b, the Ti $2p_{3/2}$ peak of the bio-TS-1 sample exhibits a shift towards lower binding energy in contrast to that of TS-1. Furthermore, the N 1s peak observed at 401.2 eV is indicative of the formation of anionic N within the O–Ti–N framework, as illustrated in Fig. 3c.[37] Based on literature reports, the incorporation of a biological template leads to the intercalation of nitrogen atoms within the bio-TS-1 framework, substituting for lattice oxygen atoms and transferring their electrons to Ti sites, thereby inducing a negative shift in binding energy.[38–40] This indicates that the self-doping of N modifies the electronic structure of Ti. However, the electronic structure of Au was not affected by N doping, as evidenced by the similar positions of the Au 4f peaks for Au/TS-1 and Au/bio-TS-1 (Fig. S4†).

In the vapor-phase epoxidation of propylene with H_2/O_2, the reactive species *OOH interacts with Ti sites, forming the intermediate Ti-OOH. This intermediate then engages the

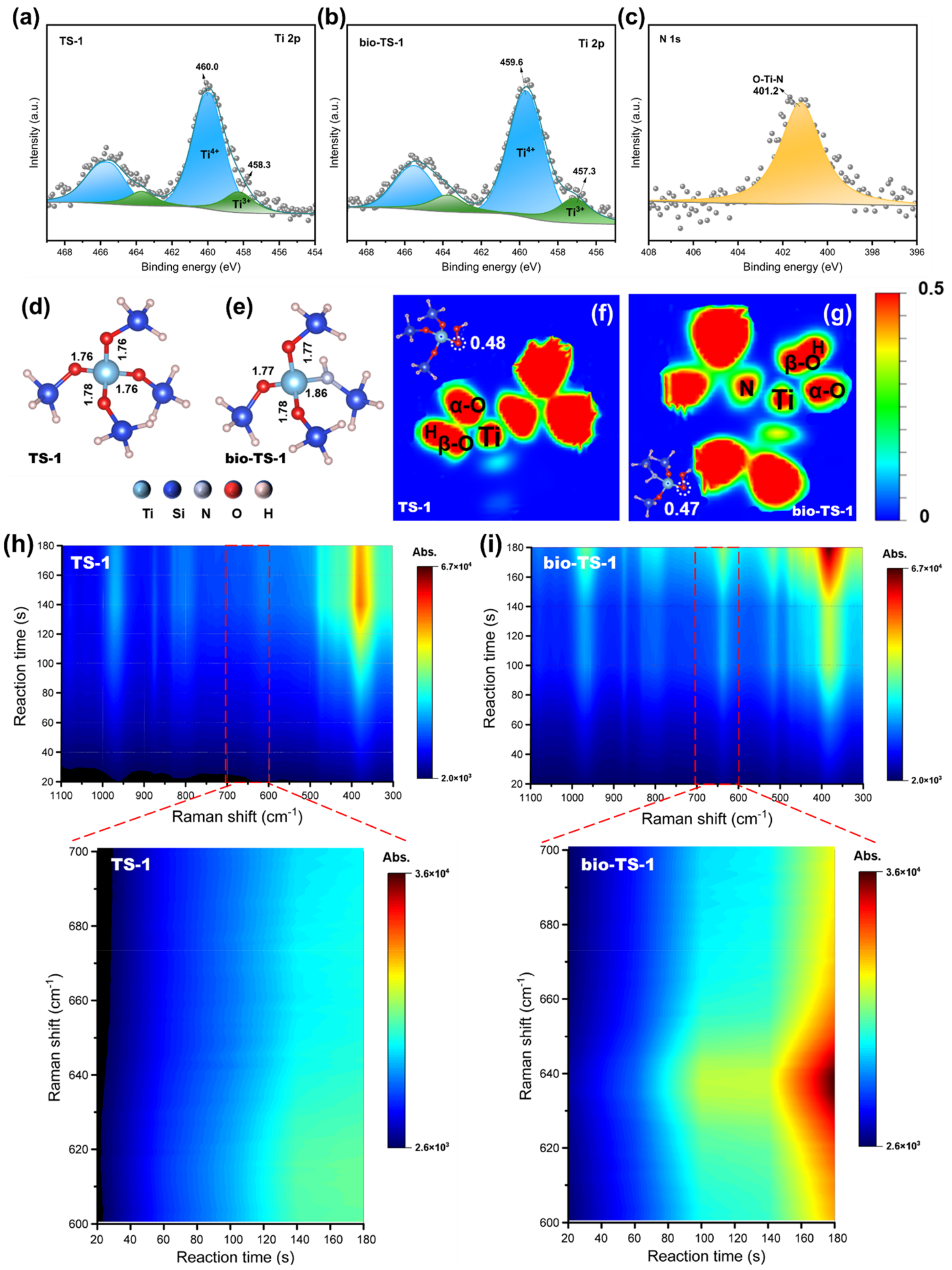

Fig. 3 (a and b) XPS spectra for Ti 2p of TS-1 and bio-TS-1. (c) N 1s of bio-TS-1. Optimized geometry and electronic localized functions (ELF) of Ti-OOH with (d and f) TS-1 and (e and g) bio-TS-1. Quasi *in situ* Raman spectra of (h) TS-1 and (i) bio-TS-1 at different exposure times.

carbon–carbon double bond (C=C) of propylene, leading to the formation of PO. Therefore, the electronic structure of the Ti sites significantly influences the epoxidation reaction. To investigate the effects of electronic structure modifications induced by N doping from pollen, we performed density functional theory (DFT) calculations. Utilizing insights from prior research and corroborated by XPS data, we selected five SiO_4 tetrahedral clusters representative of MFI-structured zeolites for computational simulation. As depicted in Fig. 3d and e, the incorporation of N alters the geometry around the Ti sites, with the elongation of all Ti–O bonds and the Ti–N bond measuring 1.86 Å, notably longer than the Ti–O bond measuring 1.76 Å. This N-insertion into the silicon framework of bio-TS-1 results in a more relaxed Ti-site configuration, potentially enhancing the accessibility for H_2O_2 to form the active Ti-OOH species.[41–43] Additionally, we examined the influence of structural alterations at the Ti sites on the reactivity of the Ti-OOH species. Our calculations, presented in Fig. 3f and 3g, reveal that the charge density of the α-O atoms in TS-1 and bio-TS-1 is 0.48 and 0.47, respectively. The diminished charge density at the α-O atoms in bio-TS-1 endows them with greater nucleophilicity towards the electron-rich C=C bond of propylene, thereby promoting the formation of more epoxide products during the reaction.[25,44]

In the quest for a more profound comprehension of the influence that electronic configuration modifications exert on reactions, the stability of the active species was evaluated through quasi *in situ* Raman spectroscopy. The Raman signal intensity is linearly correlated with the exposure duration. Prolonged exposure, however, may precipitate the cumulative thermal effects emanating from the light source, leading to the decomposition of labile components and consequently attenuating the signal peak intensities. Therefore, the stability of the active species during the epoxidation reaction can be simulated by monitoring the temporal changes in the signal intensity of the characteristic Ti-OOH peak. First, the Raman spectra of bio-TS-1, both prior to and subsequent to the introduction of hydrogen peroxide, were scrutinized, confirming that the Ti-OOH characteristic peak is positioned at 637 cm^{-1} (Fig. S5†). Thereafter, the quasi *in situ* Raman spectra (Fig. 3h and i) illustrate that the signal intensities of the bio-TS-1 sample's characteristic peaks progressively intensified with escalating exposure time. Conversely, the trend of Ti-OOH signals in TS-1 samples was not obvious, signifying that the Ti-OOH species underwent decomposition upon extended exposure (Fig. S6†). The aforementioned results indicate that the N element introduced by pollen modification has altered the electronic structure of the bio-TS-1 sample, endowing it with a stronger attraction and stability for the active species *OOH, which is crucial for the epoxidation reaction to proceed.

3.3 Catalytic performances

To underscore the structural superiority of the bio-TS-1 sample, an epoxidation reaction was conducted, with the pertinent data graphically represented in Fig. 4. Fig. 4a illustrates that the Au/bio-TS-1 catalyst outperformed its Au/TS-1 counterpart across all pivotal performance indices, a phenomenon attributed to the geometric and electronic modifications imparted by the pollen. Fig. 4b presents a statistical overview of the PO formation rate and stability data for catalysts in recent related studies.[7,11,13,32,45–49] It is evident that there is a distinct trade-off relationship between the two. A high PO formation rate leads to the accumulation of a large amount of PO within the micropores of TS-1, causing catalyst deactivation. In contrast, the hierarchical pore structure inherent to the Au/bio-TS-1 catalyst, which is templated by pollen, facilitates rapid PO desorption, enhancing catalyst stability. Even at a higher PO formation rate, no significant performance decline was observed over a 120 hour testing period. This observation implies that the multi-stage porosity can significantly influence stability by modulating the adsorption–desorption dynamics.

Furthermore, durability assessments, depicted in Fig. 4c, indicated no discernible decline in the PO formation rate, selectivity, conversion, or H_2 efficiency of Au/bio-TS-1 under continuous operational conditions. Conversely, the Au/TS-1 catalyst exhibited a precipitous drop in conversion within the initial seven hours, as highlighted in Fig. 4d. This indicates that the coking effect not only blocks the pores and occupies the adsorption sites of the reactants but also poisons the active sites on the catalyst. Moreover, the dynamic tracking of H_2O during the reaction process revealed that the Au/bio-TS-1 catalyst with Ti-OOH possesses higher activity and stability (Fig. S7†). This is attributed to the self-doping of N that modifies the Ti sites, enhancing their accessibility to OOH groups.[41–43] The lower α-O charge density and stronger nucleophilic attack on electron-rich C=C bonds are key factors contributing to the improved performance.[25,44]

3.4 Relationship of the pore structure and catalytic performance

To further elucidate the deactivation mechanism of catalysts, it is crucial to consider the accumulation of reaction products. The excessive buildup of these products can lead to the formation of carbonaceous deposits, which in turn obstruct the porous structure of catalysts. This blocking effect not only hinders the diffusion of reactants and products but also destroys the active sites and reduces the selectivity of the products, hindering industrial application of catalysts. Analysis of the N_2 adsorption–desorption isotherms (Fig. 2d) and SEM images (Fig. 1) reveals that bio-TS-1 not only mimics the morphology of a pollen template but also possesses a rich network of pore channels. Furthermore, bio-TS-1 demonstrated excellent catalytic properties, especially higher selectivity and longer lifetime. Despite these attributes, the microstructure–activity relationship of bio-TS-1 remains to be elucidated. Consequently, a series of PO adsorption–desorption experiments were conducted to elucidate the influence of the multi-stage pore structure on PO mass transfer dynamics.

As depicted in Fig. 5a, the PO breakthrough curve illustrates that due to the hierarchical pore structure of bio-TS-1, PO rapidly accumulates within its cavities and subsequently

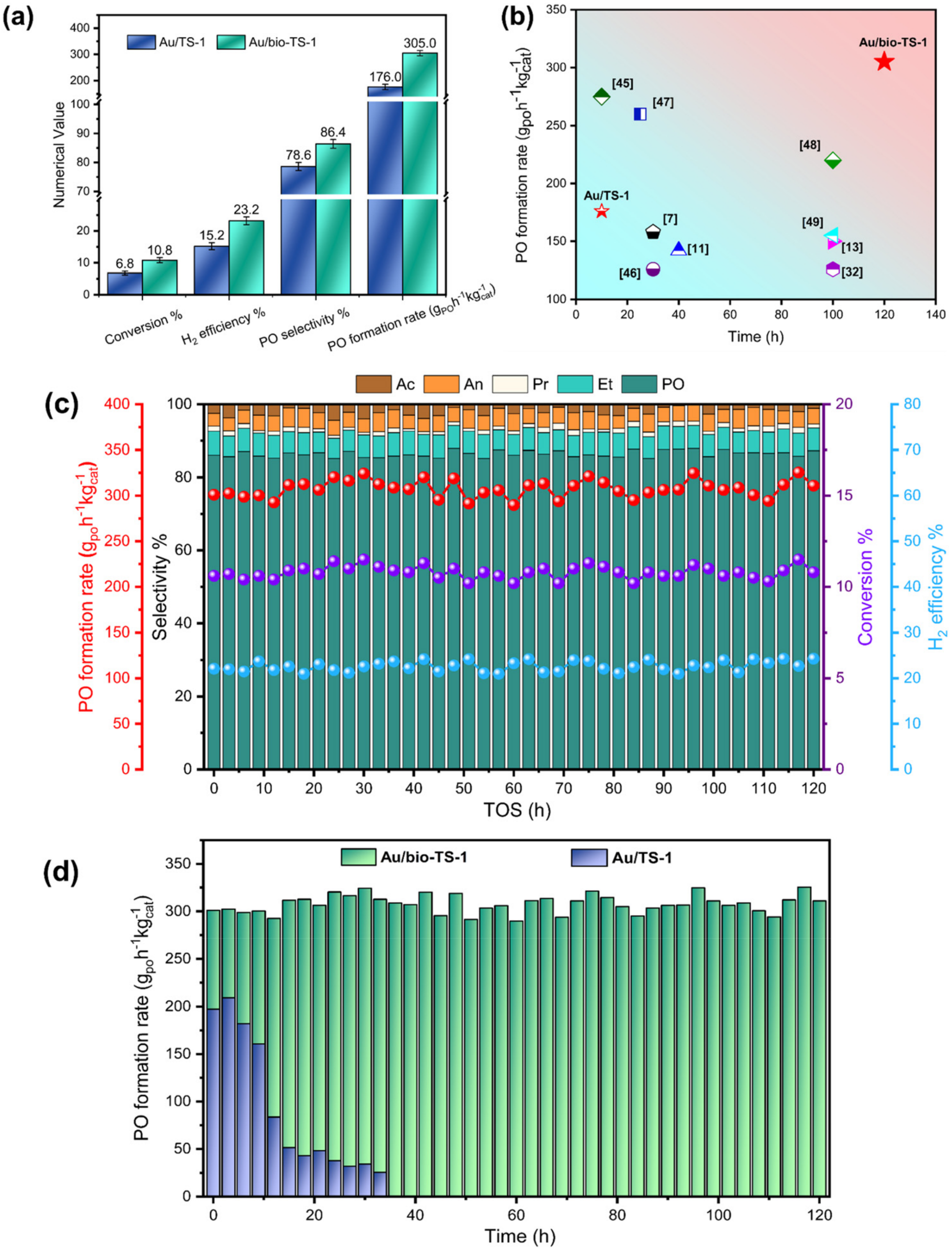

Fig. 4 (a) Catalytic performance and (b) comparison of performance between this work and recent work. (c) Stability test results of the Au/bio-TS-1 catalysts. (d) PO formation rate of Au/bio-TS-1 and Au/TS-1 catalysts (reaction conditions: $H_2/O_2/C_3H_6/Ar$ = 1/1/1/7, 200 °C, GHSV = 14 000 mL g^{-1} h^{-1}).

breaks through. In contrast, the breakthrough efficiency of TS-1 is relatively slower, indicating a significant collision and compression of PO molecules within the micropores of TS-1. After adsorption saturation, the aforementioned samples were purged with N_2. Throughout the purge desorption phase, the concentration of PO on bio-TS-1 was significantly lower than that on TS-1, and the desorption rate was faster. Towards the end of desorption, unlike bio-TS-1, there was a noticeable presence of PO molecules that were difficult to desorb from TS-1. This behavior directly leads to catalyst deactivation due to coking during the reaction process.

To further investigate the adsorption and desorption behavior of PO on two catalysts, we conducted *in situ* DRIFT experiments. As depicted in Fig. 5b and c, both catalyst surfaces exhibited combined signals in the regions of 2800–3000 cm^{-1} and 3600–3800 cm^{-1} upon PO purging. The former is attributed to the stretching vibrations of the C–H bonds in PO, while the inverted peak in the latter region is due to the coverage of Ti-OH sites by the methoxy group of PO.[9,22,50] Compared to bio-TS-1, TS-1 exhibited a significantly stronger C–H signal. Furthermore, an inverted peak was observed at the sixth minute for TS-1, whereas a distinct inverted peak in bio-TS-1

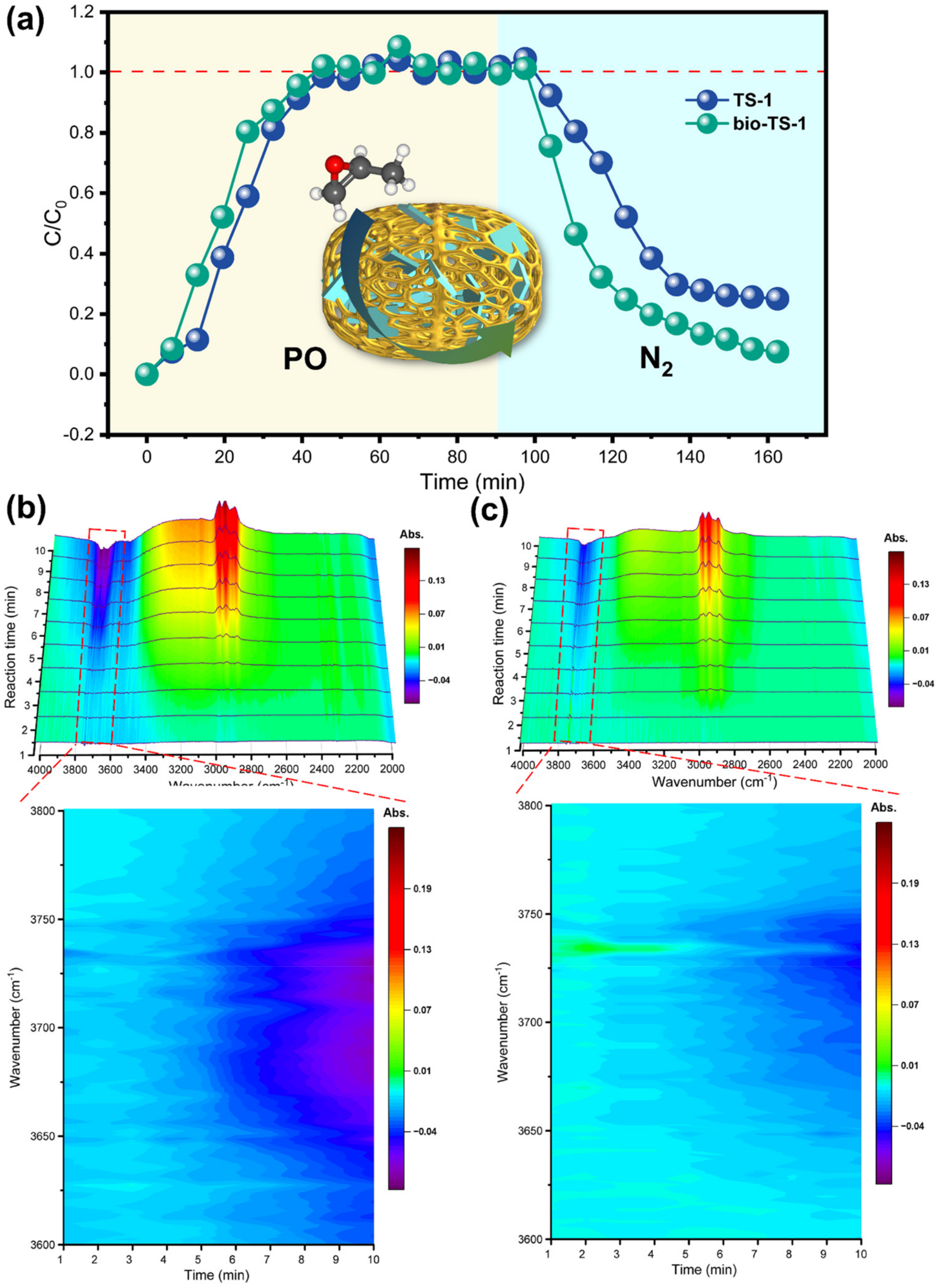

Fig. 5 (a) PO breakthrough curves and *in situ* PO-DRIFT of (b) TS-1 and (c) bio-TS-1.

appeared only at the ninth minute. This suggests that the adsorption of PO on TS-1 is more pronounced, while PO on bio-TS-1 is capable of timely desorption. Incorporating our findings from the PO adsorption and desorption studies, we deduce that the bio-TS-1, synthesized using a pollen template, not only retains the intrinsic microporosity of the zeolite but also introduces a significant array of intergranular mesopores and macropores. This distinctive hierarchical pore architecture diminishes the intra-zeolitic diffusion length for the products, thereby facilitating the rapid desorption of PO produced in the reaction. This enhanced desorption capacity is pivotal in curtailing the formation of by-products, thereby enhancing both the selectivity towards PO and the overall stability of the catalyst.

4. Conclusion

In summary, we have successfully synthesized a bio-TS-1 catalyst using pollen as a template, which effectively retains the unique hierarchical porous structure inherent to biomass materials. PO breakthrough curves and *in situ* DRIFT have confirmed that this innovation enhances mass transfer efficiency and facilitates product desorption, effectively addressing the issues of carbon deposition that is characteristic of traditional TS-1 catalysts, which are constrained by their single microporous structure. Interestingly, the pollen template not only imparts a multi-level porous structure but also modulates the electronic structure of the catalyst. The DFT calculations and quasi *in situ* Raman spectroscopy have revealed that this electronic effect enhances the activity and stability of the Ti-OOH active sites. The Ti sites are more relaxed and the α-O in Ti-OOH is more aggressive towards C═C bonds of propylene. The synergistic effect breaks the trade-off between performance and stability, with not only the PO yield reaching up to 305 g_{PO} h^{-1} $kg_{cat}{}^{-1}$ but also the catalyst exhibiting stability for over 120 h. This study not only presents a superior epoxidation catalyst but also, more importantly, offers a novel perspective for the synthesis of hierarchically porous zeolites.

Author contributions

Shaodi Sun: methodology, formal analysis, writing, and editing. Yichen Liao: conceptualization, investigation, writing, and editing. Zhuang Wang: editing. Chuanhu Wang: DFT calculations. Daohua Sun: supervision, funding acquisition, and guidance.

Data availability

The data that support the findings of this study are available from the corresponding author upon reasonable request.

Conflicts of interest

The authors declare no competing financial interest.

Acknowledgements

The author sincerely appreciates the financial support from the National Natural Science Foundation of China (22078269).

References

1 T. Hayashi, K. Tanaka and M. Haruta, *J. Catal.*, 1998, **178**, 566–575.
2 W.-S. Lee, M. Cem Akatay, E. A. Stach, F. H. Ribeiro and W. Nicholas Delgass, *J. Catal.*, 2012, **287**, 178–189.
3 S. J. Khatib and S. T. Oyama, *Catal. Rev.*, 2015, **57**, 306–344.
4 A. K. Sinha, S. Seelan, S. Tsubota and M. Haruta, *Angew. Chem., Int. Ed.*, 2004, **43**, 1546–1548.
5 W. Cheng, X. Wang, G. Li, X. Guo and S. Zhang, *J. Catal.*, 2008, **255**, 343–346.
6 J. Huang, T. Takei, T. Akita, H. Ohashi and M. Haruta, *Appl. Catal., B*, 2010, **95**, 430–438.
7 X. Feng, X. Duan, J. Yang, G. Qian, X. Zhou, D. Chen and W. Yuan, *Chem. Eng. J.*, 2015, **278**, 234–239.
8 B. S. Uphade, T. Akita, T. Nakamura and M. Haruta, *J. Catal.*, 2002, **209**, 331–340.
9 A. Ruiz, B. Van Der Linden, M. Makkee and G. Mul, *J. Catal.*, 2009, **266**, 286–290.
10 H. Wang and T. J. Pinnavaia, *Angew. Chem., Int. Ed.*, 2006, **45**, 7603–7606.
11 X. Feng, N. Sheng, Y. Liu, X. Chen, D. Chen, C. Yang and X. Zhou, *ACS Catal.*, 2017, **7**, 2668–2675.
12 Y. Li, Q. Fan, Y. Li, X. Feng, Y. Chai and C. Liu, *Appl. Surf. Sci.*, 2019, **483**, 652–660.
13 N. Sheng, Z. Liu, Z. Song, D. Lin, X. Feng, Y. Liu, X. Chen, D. Chen, X. Zhou and C. Yang, *Chem. Eng. J.*, 2019, **377**, 119954.
14 G. Yang, J. Han, Z. Qiu, X. Chen, Z. Feng and J. Yu, *Inorg. Chem. Front.*, 2020, **7**, 1975–1980.
15 M. W. Anderson, S. M. Holmes, N. Hanif and C. S. Cundy, *Angew. Chem., Int. Ed.*, 2000, **39**, 2707–2710.
16 X. Li, T. Fan, H. Zhou, S. Chow, W. Zhang, D. Zhang, Q. Guo and H. Ogawa, *Adv. Funct. Mater.*, 2009, **19**, 45–56.
17 L. Qin, M. Liu, Y. Wu, Z. Xu, X. Guo and G. Zhang, *Appl. Catal., B*, 2016, **194**, 50–60.
18 B. Sun, T. Fan, J. Xu and D. Zhang, *Mater. Lett.*, 2005, **59**, 2325–2328.
19 S. R. Hall, V. M. Swinerd, F. N. Newby, A. M. Collins and S. Mann, *Chem. Mater.*, 2006, **18**, 598–600.
20 F. Song, H. Su, J. Han, W. M. Lau, W.-J. Moon and D. Zhang, *J. Phys. Chem. C*, 2012, **116**, 10274–10281.
21 J. Zhao, D. Wei, X. Zhang, S. Zhang, C. Zhang and X. Yang, *J. Colloid Interface Sci.*, 2022, **606**, 577–587.
22 S. Yao, L. Xu, J. Wang, X. Jing, T. Odoom-Wubah, D. Sun, J. Huang and Q. Li, *Mol. Catal.*, 2018, **448**, 144–152.
23 X. Gao and I. E. Wachs, *Catal. Today*, 1999, **51**, 233–254.
24 M. H. Mahyuddin, A. Staykov, Y. Shiota and K. Yoshizawa, *ACS Catal.*, 2016, **6**, 8321–8331.
25 L. Wang, Y. Xu, G. Zhai, Y. Zheng, J. Huang, D. Sun and Q. Li, *ACS Sustainable Chem. Eng.*, 2020, **8**, 12177–12186.
26 G. Kresse and D. Joubert, *Phys. Rev. B: Condens. Matter Mater. Phys.*, 1999, **59**, 1758–1775.
27 J. P. Perdew, K. Burke and M. Ernzerhof, *Phys. Rev. Lett.*, 1996, **77**, 3865–3868.
28 A. D. Becke and K. E. Edgecombe, *J. Chem. Phys.*, 1990, **92**, 5397–5403.
29 V. Wang, N. Xu, J.-C. Liu, G. Tang and W.-T. Geng, *Comput. Phys. Commun.*, 2021, **267**, 108033.
30 J. Zhao, S. Ge, L. Liu, Q. Shao, X. Mai, C. X. Zhao, L. Hao, T. Wu, Z. Yu and Z. Guo, *Ind. Eng. Chem. Res.*, 2018, **57**, 231–241.
31 R. B. Khomane, B. D. Kulkarni, A. Paraskar and S. R. Sainkar, *Mater. Chem. Phys.*, 2002, **76**, 99–103.
32 Z. Song, X. Feng, N. Sheng, D. Lin, Y. Li, Y. Liu, X. Chen, D. Chen, X. Zhou and C. Yang, *Chem. Eng. J.*, 2019, **377**, 119927.

33 T. Zhang, X. Chen, G. Chen, M. Chen, R. Bai, M. Jia and J. Yu, *J. Mater. Chem. A*, 2018, **6**, 9473–9479.

34 Y. Wang, H. Yang, Y. Zuo, D. Tian, G. Hou, Y. Su, Z. Feng, X. Guo and C. Li, *Appl. Catal., B*, 2023, **325**, 122396.

35 W. Xu, T. Zhang, R. Bai, P. Zhang and J. Yu, *J. Mater. Chem. A*, 2020, **8**, 9677–9683.

36 S. Mintova, M. Hölzl, V. Valtchev, B. Mihailova, Y. Bouizi and T. Bein, *Chem. Mater.*, 2004, **16**, 5452–5459.

37 A. Azarniya, M. Zekavat, M. Soltaninejad, F. Bakhshandeh, H. Reza Madaah Hosseini, S. Kashani, C. Amutha, S. Khatiboleslam Sadrnezhaad and S. Ramakrishna, *Adv. Powder Technol.*, 2020, **31**, 3328–3341.

38 X. Jiang, Y. Liu, H. Hao, Y. Xu, J. Huang, D. Sun and Q. Li, *ACS Sustainable Chem. Eng.*, 2018, **6**, 882–888.

39 H. Li, Q. Lei, X. Zhang and J. Suo, *Microporous Mesoporous Mater.*, 2012, **147**, 110–116.

40 T. Yuan, Q. Zhu, L. Gao, J. Gao and W. Ma, *J. Mater. Sci.*, 2020, **55**, 3803–3811.

41 X. Fang, L. Wu, Y. Yu, L. Sun and Y. Liu, *Catal. Commun.*, 2018, **114**, 1–5.

42 M. Wu, H. Song, F. Wang and L. Chou, *J. Mol. Catal. Chem.*, 2013, **379**, 207–212.

43 H. Munakata, Y. Oumi and A. Miyamoto, *J. Phys. Chem. B*, 2001, **105**, 3493–3501.

44 T. Liu, P. Hacarlioglu, S. T. Oyama, M.-F. Luo, X.-R. Pan and J.-Q. Lu, *J. Catal.*, 2009, **267**, 202–206.

45 Z. Zhang, S. Shi, Y. Tang, J. Xu, W. Du, Q. Wang, D. Yu, Y. Liao, N. Song, X. Duan and X. Zhou, *J. Catal.*, 2022, **416**, 410–422.

46 X. Feng, X. Duan, G. Qian, X. Zhou, D. Chen and W. Yuan, *Appl. Catal., B*, 2014, **150–151**, 396–401.

47 W.-S. Lee, M. Cem Akatay, E. A. Stach, F. H. Ribeiro and W. Nicholas Delgass, *J. Catal.*, 2013, **308**, 98–113.

48 D. Lin, X. Zheng, X. Feng, N. Sheng, Z. Song, Y. Liu, X. Chen, Z. Cai, D. Chen and C. Yang, *Green Energy Environ.*, 2020, **5**, 433–443.

49 Z. Song, H. Yan, J. Yuan, H. Ma, J. Cao, Y. Wang, Q. Wang, C. Peng, F. Deng, X. Feng, D. Chen, C. Yang and Y. Hu, *Engineering*, 2023, **25**, 144–156.

50 G. Mul, A. Zwijnenburg, B. Van Der Linden, M. Makkee and J. A. Moulijn, *J. Catal.*, 2001, **201**, 128–137.